

Optical and Electrical Properties of Nanostructured Metallic Electrical Contacts

Victor J. Toranzos and Guillermo P. Ortiz

Departamento de Física - Facultad de Ciencias Exactas Naturales y Agrimensura,
Universidad Nacional del Nordeste, Corrientes, Argentina.
gortiz@exa.unne.edu.ar

W. Luis Mochán

*Instituto de Ciencias Físicas,
Universidad Nacional Autónoma de México,
Cuernavaca, Morelos, México*

Jorge O. Zerbino

Instituto de Investigaciones Fisicoquímicas Teóricas y Aplicadas
Centro Investigaciones Científicas de la Provincia de Buenos Aires, La Plata, Argentina.

We study the optical and electrical properties of silver films with a graded thickness obtained through metallic evaporation in vacuum on a tilted substrate to evaluate their use as semitransparent electrical contacts. We measure their ellipsometric coefficients, optical transmissions and electrical conductivity for different widths, and we employ an efficient recursive method to calculate their macroscopic dielectric function, their optical properties and their microscopic electric fields. The topology of very thin films corresponds to disconnected islands, while very wide films are simply connected. For intermediate widths the film becomes semicontinuous, multiply connected, and its microscopic electric field develops hotspots at optical resonances which appear near the percolation threshold of the conducting phase, yielding large ohmic losses that increase the absorptance above that of a corresponding homogeneous film. Optimizing the thickness of the film to maximize its transmittance above the percolation threshold of the conductive phase we obtained a film with transmittance $T = 0.41$ and a sheet resistance $R_{\square}^{\max} \approx 2.7\Omega$. We also analyze the observed emission frequency shift of porous silicon electroluminescent devices when Ag films are used as solid electrical contacts in replacement of electrolytic ones.

I. INTRODUCTION

Transparent electric contacts are needed in a widespread variety of optoelectronic applications. Materials such as coinable metals are very good electrical conductors when compared to the conductive polymers or semiconductor materials often used for those applications,¹ but unfortunately, they are opaque. Organic conductive materials and doped metallic oxides have been considered a good compromise, behaving as conductors at low frequency and as dielectrics at optical frequencies.¹ Nonetheless, the properties of these semiconductor materials are defined by their chemical composition and their doping. Thus, tuning the threshold frequency at which they change behavior from conductor to dielectric is difficult. An alternative for the design of semitransparent electrical contacts is the use of nanostructured metallic-dielectric composites. Extraordinary optical transmission² in perforated metallic films with nanoporations has been explained in terms of bulk and surface plasmons in nanostructured films³ and is promising for the control of optical properties.⁴ These systems, are composed of a metallic and a dielectric phase; one of them may be described as an array of nanometric inclusions with a given geometry. Material composition, geometry, and order, affect the optical properties of the system.^{5,6} Fabrication of nanostructured films with ordered patterns designed to tune optical properties in the visible (VIS) range requires high resolution lithography, employing interferometry of electronic beams^{7,8} or similar techniques. A relative

simple alternative is to use random composite films.⁹ Unlike the metallic oxides, this kind of semitransparent contacts do not require high temperatures, are flexible, might possess low enough surface roughness for the optical range, and have a relatively low cost of production.

It is well known that the optical transmission⁹ as well as the electrical resistivity¹⁰ of uniform metallic thin films increase as the films becomes thinner. However, the reduction of the thickness of a film usually modifies its morphology leading to inhomogeneities. A thin enough film is made of separate *islands*¹¹ and is therefore non-conducting. Near but above the percolation threshold, while the conductive phase is connected, there appear optical resonances at which the transmittance is suppressed due to the power dissipated as Joule heat.¹² In the present work, we employ a computationally efficient recursive formalism for the calculation of an effective dielectric response of nanostructured films when the length-scale of the inhomogeneities of the film are much smaller than the wavelength, thus neglecting retardation.^{5,6,13} This non-retarded recursive method (RM) is applicable¹⁴ to nano-textured inhomogeneities with scales up to one order of magnitude below the nominal wavelength. Analyzing the optical and electrical properties of semicontinuous Ag films with a graded thickness we have searched for an optimum film, with an adequate conductivity in the low frequency range and a relatively high transmittance in the VIS.

We also study Ag electrical contacts on porous silicon (PS) electro-luminescent devices (ELD). It is known¹⁵ that in

metal/PS/cSi junctions under a bias voltage the injected carriers may recombine. Due to the quantum confinement within the thin Si regions in PS, direct radiative transitions with an energy larger than the bulk indirect gap become permitted, leading to electro-luminescence (EL) in the VIS range of the spectrum. Photo luminescence (PL) may also be observed if the sample is irradiated by ultraviolet (UV) light. A relation between the PL spectra with the porosity p and the morphology of PS was proposed by Bessaï et al.¹⁶, yielding a maximum emission at 680nm with $p=0.8$. Under similar preparation conditions, the PL and EL spectra are expected to be similar¹⁷. EL spectra from PS excited through an electrolytic contact¹⁸ have been characterized as a function of the excitation potential and electric current, allowing the control of the emission spectra through the preparation condition. However, it has been found that the EL spectra of similarly prepared PS films samples differ when they are excited through different solid contacts. For PS with an expected porosity around 80% over p doped Si with Au vacuum evaporated contacts (Au/PS/ p -Si/Al), a peak emission was obtained at 680.¹⁹ Similarly for an ITO contact¹⁹ or for an Al contact and an n doped substrate (Al/PS/ n -Si/Al).¹⁷ Nevertheless, for an Au contact prepared by sputtering (Au/PS/ p -Si/Al) the EL peak shifts to 560nm²⁰. Other shifts have been reported for contacts made through the co-evaporation of Au and Ga or Sn (530nm), Au and In (455nm), and Au and Sb (700nm).²¹ In the above cases the intensity of the EL signal was strongly suppressed.

In this paper we also explore experimentally and theoretically the spectral shift and the intensity suppression of the EL signal when an electrolytic contact over an PS-ELD is replaced by a solid Ag contact.

The paper is organized as follows: In section II we present our method for fabricating Ag films with variable thickness in only one evaporation step (subsection II A), and we discuss our procedures for measuring the transmittance, ellipsometric coefficients and resistance (II B). In section III we discuss our model for the semicontinuous film and we describe our computational procedures. In section IV we obtain theoretical results from the RM for the ellipsometric coefficients (IV A), the electrical properties(IV B), and the transmittance (IV C) of semicontinuous films. As an application, in section V we fabricate an optimally tuned solid transparent electrical contact (V A) and we propose an explanation for the spectral shift and the suppression of the observed emission of a PS-ELD (subsec. V B). We devote section VI to conclusions.

II. EXPERIMENTAL

In this section we describe the experimental setup employed to determine the optimal thickness of thin metallic films by fabricating samples with a graded thickness and measuring their optical transmittance, ellipsometric coefficients, and four-point electrical resistance. The optimal thickness would be the one that maximizes the transmittance and minimizes the resistance.

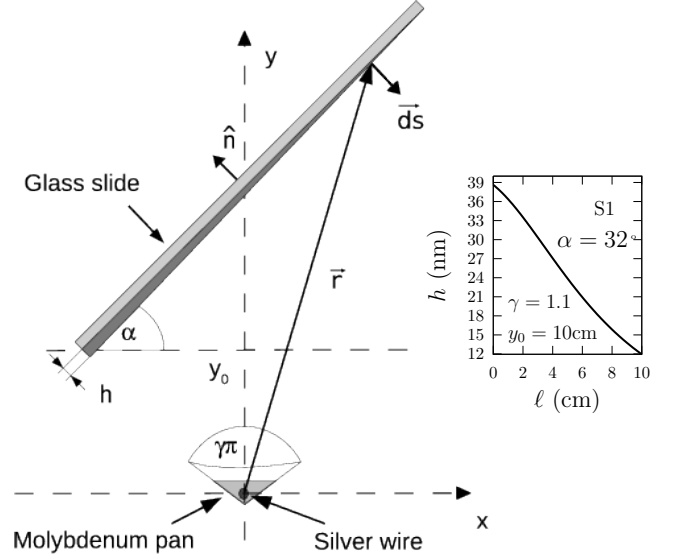


FIG. 1. Experimental setup for the growth of films with a graded thickness using a coinable-metal vacuum evaporation technique. A molybdenum crucible with an aperture that spans a solid angle $\gamma\pi$ supports a small piece of Ag wire that is melted and vaporized by contact with an electrical heating device (not shown). The sample with variable thickness (dark gray) is grown on a glass slide (light gray) tilted an angle α . We indicate a differential element of surface $d\vec{s} = -ds \hat{n}$ at position \vec{r} , and the height y_0 of the lower edge of the slide. Inset: Nominal height h versus position ℓ along the sample calculated from α , y_0 , m and γ for sample S1.

A. Sample Preparation

Fig.1 displays our setup for growing film samples with a graded thickness (h), adapted from a coinable-metal vacuum evaporation technique.^{22,23} The sample is obtained by isotropic thermal evaporation of Ag through a solid angle $\gamma\pi$ determined by the aperture of a conical molybdenum crucible whose walls screen the lower part of a vacuum bell device. On a surface element $d\vec{s}$ at position \vec{r} on a glass slide, the deposited mass dm is given by $-m\hat{r} \cdot d\vec{s}/(\gamma\pi r^2)$ where m is the total Ag mass vaporized. A nominal width h may be obtained by dividing the mass per unit area of the film by the bulk mass density of Ag. The actual density may be smaller and the actual width larger due to texture of the film. Due to the inclination α of the slide with respect to the horizontal, the deposited film is thicker on the side that is closer to the source, at a height y_0 above the crucible, and thinner on the opposite side. Thus, we can prepare samples with variable thickness within a range that depends on the geometrical parameters of the experimental setup. We show below results for two samples, both prepared with $\gamma = 1.1$, sample S1 with $y_0 = 10$ cm, $\alpha = 32^\circ$, $m = 16.5$ mg and sample S2 with $y_0 = 9.7$ cm, $\alpha = 42^\circ$, and $m = 8.25$ mg. The inset of Fig.1 shows the thickness h as a function of position ℓ along the sample S1.

B. Optical and electrical properties

We measured and averaged the optical normal-incidence transmittance along three parallel equispaced lines running longitudinally through the sample in the gradient direction, using (a) a 650 nm diode laser with a spot of diameter 1.5 mm, and (b) an Ocean Optics UV-NIS-NIR source through an optical fiber. In both cases we measured the intensity of the transmitted light at $\Delta\ell = 5\text{mm}$ intervals. We used a clean glass slide as a reference. For (a) we used a detector based on a photo-diode BPW20RF and in (b) the data were collected from a USB spectrometer and we employed the *Spectrasuite* software. We also determined the sheet resistance R_\square over the same places using a four-point technique.^{22,24}

We measured the ellipsometric parameters of the sample ψ and δ , defined through

$$\frac{r_p}{r_s} = \exp(i\delta) \tan(\psi), \quad (1)$$

where r_p and r_s are the reflection coefficients for p and s polarization, respectively, with a Rudolph Research type 43702-200E ellipsometer in the null field mode.²⁵ We fixed the incidence angle θ , we put a linear polarizer and a quarter wave plate across the incident beam oriented at angles P and C with respect to the plane of incidence, respectively, and a linear analyzer across the reflected beam at an angle A . We set $C = \pi/4$ and found $\delta = 2P + \pi/2$, and $\psi = A$ for different film thicknesses and wavelengths, where we choose P and A to minimize the intensity of the outgoing beam.

III. MODEL

For very thin films of coinable metals an *island* morphology type has been reported.^{4,10} As the film grows the islands eventually connect among themselves, leading to a semicontinuous film textured in the nanometric scale.^{10,11,26} For thickness smaller than a couple dozen nanometers, the air interstices among the islands may sustain resonant excitations that significantly modify the optical^{5,6} and electrical²⁷ properties. As we move along our graded sample towards its thick edge those islands become more connected and for very thick films they merge into a continuous film. Fig. 2 shows schematically the proposed morphology. Our model consists of an ensemble of periodically repeated unit cells, each of which contains a large enough number of penetrable disks of radius a and height h_d occupying random uncorrelated positions. The ensemble is characterized by the filling fraction f , i.e., the fraction of the area covered by the metal, and the amount of metal deposited per unit area, which in turn is characterized by the nominal height h . We employed the RM to calculate the macroscopic dielectric function ϵ^M of the composite^{5,6,14} using the *Photonic* package.¹³ The filling fraction f may be adjusted in the model by varying the radius a of the disks and the height h_d is related to f through $h_d = h/f$.

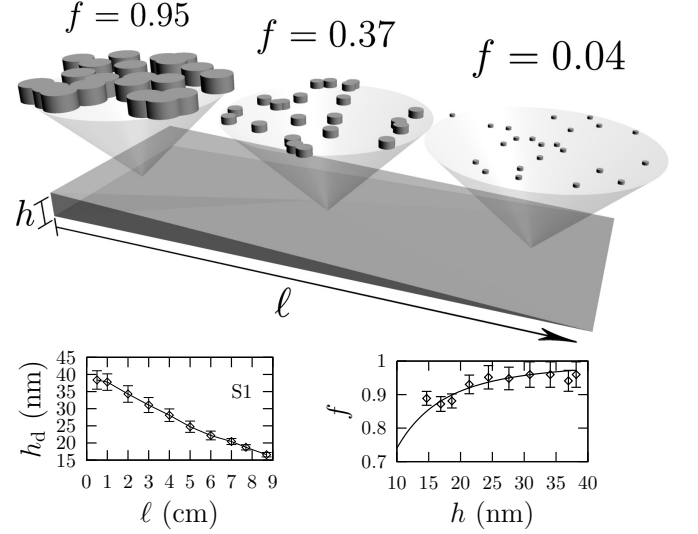


FIG. 2. Model film morphology at different positions ℓ along a sample prepared as in Fig. 1. The smooth wedge illustrates the nominal geometry, while the amplified regions illustrate our model, consisting of an ensemble of penetrable Ag disks of radius a and height h_d at uncorrelated random positions, yielding a semicontinuous film with filling fraction f . Below: Height of the disks h_d as a function of position ℓ and filling fraction f as a function of nominal height h as adjusted to the ellipsometric measurements (see text).

IV. RESULTS

A. Ellipsometric coefficients

We measured the ellipsometric coefficients at a fixed incidence angle $\theta = 69^\circ$. We measured δ and ψ at ten different positions ℓ along sample *S1* and five wavelengths $\lambda = 405, 451, 492, 546$ and 580nm . In the left panel of Fig. 3 we show our results for three of those (we omitted two to avoid cluttering the figure). Each point in Fig. 3 corresponds to a different thickness h (ψ increases with h). For thick films (above 20 nm) experiment agrees roughly with the values of ψ and δ calculated for a locally homogeneous film of width h with a dielectric function ϵ_{Ag} taken from Ref. 28 (commonly used for studying optical properties of Ag composites at frequencies in UV-VIS-NIR range) and deposited over glass, with dielectric response obtained from Ref. 29, but they don't agree for thinner films ($h < 20\text{nm}$) for which the film inhomogeneities lead to a strong dependency of the optical response with the film morphology. For each value of ℓ and h we used our model (Subsec. III) to obtain the macroscopic response of the film and identifying the width of the film with the height h_d of the disks we calculated the ellipsometric coefficients. To this end we averaged our results over a thousand realizations of our ensemble with thirty disks randomly situated within a square unit cell. We have verified convergence of the results. Our

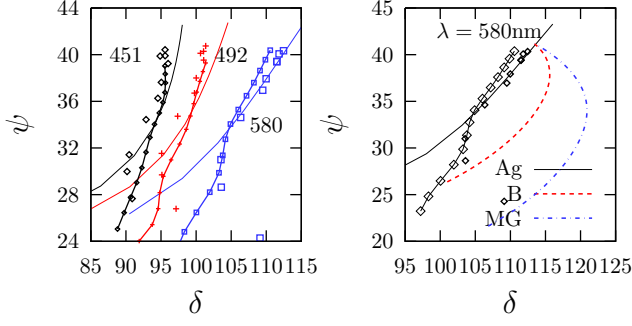


FIG. 3. Left panel: Ellipsometric coefficients (δ , ψ) for three wavelengths $\lambda = 451$ (\diamond), 492 ($+$) and 580 nm (\square) and for ten values of the thickness h (ψ increases with h for each λ). The solid lines correspond to homogeneous Ag films, and the lines with points to the RM results. Right panel: Ellipsometric coefficients measured for a wavelength $\lambda = 580$ nm and ten different thicknesses (\diamond), calculated for homogeneous films (solid lines), with RM (points with lines), and with other effective media models: Bruggeman (B, dashed lines) and Maxwell-Garnett (MG, dash-dotted lines).

model has only one parameter, namely, the radius a of the disks, and it is adjusted for each value of ℓ with corresponding nominal width h , to best reproduce the ellipsometric measurements at the five wavelengths mentioned above. Fig. 2 displays the fitted values of h_d at the ten positions ℓ for which we measured δ and ψ . It also displays the resulting filling fraction f as a function of the nominal height h , together with an analytical fit, for which we chose the form

$$f = \frac{\mu h}{\sqrt{1 + (\mu h)^2}}, \quad (2)$$

as it is linear for thin films and saturates at $f = 1$ for very thick ones. We obtained the parameter $\mu = 0.11 \text{ nm}^{-1}$.

The left panel of Fig. 3 shows that results of our RM calculation agree with experiment for most of the film thicknesses explored. In contrast, the effective medium models of Maxwell-Garnett (MG) and Bruggeman (B)³⁰ differ strongly, as shown in the right panel of Fig. 3 corresponding to $\lambda = 580$ nm. Thus, our model system and the RM computational procedure are much better suited for the calculation of the effects of the nanometric texture on optical properties of very thin films. It has been reported^{10,11} that optical properties of inhomogeneous films (such as semicontinuous film of coinable metals) differ from those of homogeneous films. However, to our knowledge, this is the first time that semicontinuous Ag films are analyzed and that the differences between homogeneous and inhomogeneous films are calculated and compared to those measured on a single sample consisting of a film with a graded thickness. This kind of analysis allows correlation of the parameters needed to design and manufacture semicontinuous films with optimal parameters.

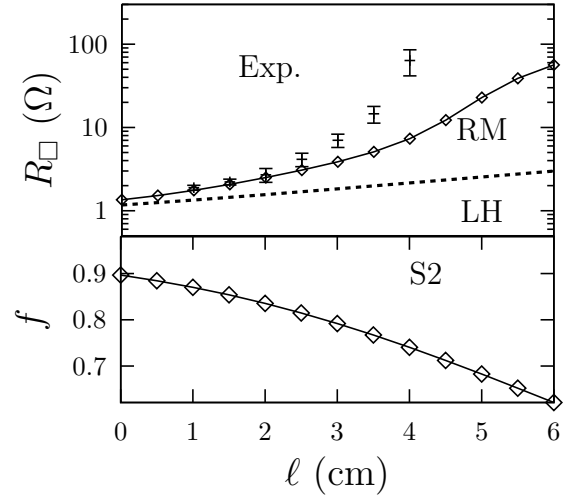


FIG. 4. Sheet resistance R_{\square} measured for sample $S2$ (crosses with error bars) as a function of position ℓ along the sample (top panel). We also show the results ρ^M/h_d calculated with the RM theory for the morphology illustrated in Fig. 2 (diamonds with lines) and the results ρ_{Ag}/h for a locally homogeneous Ag film (dashed line). In the bottom panel we include the calculated filling fraction f as a function of position ℓ .

B. Resistance

In Fig. 4 we show our measurements of the sheet resistance R_{\square} at various positions ℓ on sample $S2$, prepared with a larger angle α and a smaller mass m than sample $S1$, so that for each position ℓ the corresponding film is thinner. We also show the filling fraction calculated for each ℓ , using Eq. (2) (fitted to the ellipsometric parameters of sample $S1$) and using the nominal height h as a function of ℓ as described in Subsec. II A. Notice that the resistance increases very fast as ℓ increases, the film becomes thinner, and the filling fraction of the metal diminishes, indicative of the approach to a percolation transition at $f_c \approx 0.7$ where the resistance would diverge (we couldn't measure the resistance for filling fractions smaller than 0.74). In sample $S2$ this region corresponds roughly to the center of the sample, whereas in sample $S1$ it is too close to one of its edges, difficulting its measurement.

From the filling fraction f and the nominal height h we obtained the height h_d of our model disks. This allows us to calculate the resistivity

$$\rho^M = \frac{4\pi}{\lim_{\omega \rightarrow 0} \omega \text{Im} \{ \epsilon^M(\omega) \}}, \quad (3)$$

and the sheet resistance $R_{\square} = \rho^M/h_d$ using the RM model. To that end, we extrapolate the dielectric function of the metallic phase towards low frequencies using the Drude model

$$\epsilon_{\text{Ag}} = 1 - \frac{\omega_p^2}{\omega^2 + i\omega\gamma}. \quad (4)$$

with parameters $\hbar\gamma = 0.021 \text{ eV}$,⁴ $\hbar\omega_p = 8.51 \text{ eV}$, which correspond to the resistivity $\rho_{\text{Ag}} = 2.16 \times 10^{-6} \Omega\text{cm}$ which we

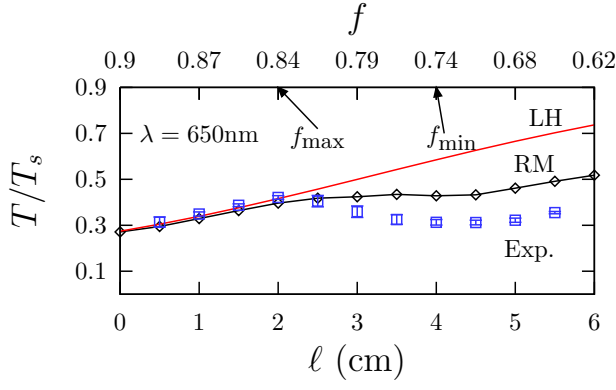


FIG. 5. Transmittance T versus position ℓ along the sample $S2$ at wavelength $\lambda = 650\text{nm}$ normalized to the transmittance T_s of the substrate. We show experimental (Exp) results and results calculated through the RM theory (RM) for the morphology illustrated in Fig. 2 and for a (locally) homogeneous film (LH). The corresponding filling fractions are indicated in the top axis.

measured for the same Ag wire from which the samples were prepared.

The theoretical results are displayed in Fig. 4. Notice that they also increase rapidly as ℓ increases, though not as rapidly as experiment. We recall that the geometrical percolation threshold for penetrable disks is $f_c = 0.676$ ³¹ and that our calculations are done on a system made up of a periodically repeated finite random unit cell so that we expect finite size effects to wash away the percolation transition in our calculation. In the same figure we also include the sheet resistance ρ_{Ag}/h of a continuous film. Its behavior is qualitatively different from both experiment and our calculation. Of course, for small ℓ and high filling fractions both models coincide and agree with experiment.

C. Transmittance

Fig. 5 displays the transmittance T normalized to the transmittance T_s of the glass slide as function of position ℓ , and thus, as a function of the filling fraction f , measured at $\lambda=650\text{nm}$ for sample $S2$. We also show the transmittance calculated with the RM model and the result for a homogeneous film.

As ℓ increases and f decreases the experimental transmittance increases up to a local maximum $T = 0.41$ corresponding to a filling fraction $f_{\text{max}} \approx 0.84$ for which the film is conducting as it lies above the percolation threshold $f_c \approx 0.7$ displayed in Fig. 4. Afterwards, T diminishes and reaches a local minimum $T = 0.29$ at $f_{\text{min}} \approx 0.74 \gtrsim f_c$. As the filling fraction diminishes further, the transmittance of the film increases again, but for $f < f_c$ the film is no longer conducting. The RM calculation does not show the maximum and minimum discussed above, but displays a similar inflection, and it follows the experimental results much more closely than the calculation for a homogeneous film.

The optical properties close to the percolation threshold de-

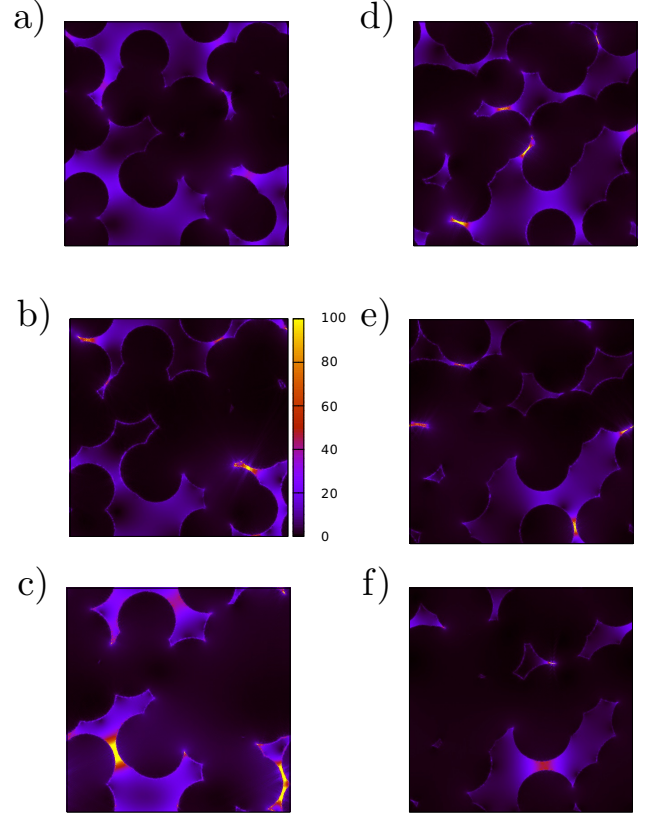


FIG. 6. Absolute value $|\vec{E}|$ of the microscopic field normalized to that of the incident field $|\vec{E}_0|$ calculated with the RM model at $\lambda = 650\text{nm}$ for two members (left and right columns) of the ensemble and for three different radii and average filling fractions $a = 0.11$, $f \approx 0.69$ (a, d), $a = 0.12$, $f \approx 0.75$ (b, e), and $a = 0.13$, $f \approx 0.81$ (c, f).

pend strongly on the morphology and on the wavelength. In this region field fluctuations are very intense and localized optical resonances known as *hotspots* occur. To illustrate the hotspots, in Fig. 6 we show the microscopic field obtained through a recursive procedure based in the RM calculation of the response.^{13,32} We show the field for two different members of the random ensemble that models the morphology of the system, and for three disk radii $a = 0.11, 0.12, 0.13$, corresponding to the averaged filling fractions $f \approx 0.69, 0.75, 0.81$, at a single wavelength $\lambda = 650\text{nm}$. Fig.6c) displays hotspots in the interstice between two nearby particles (bottom left) and between three particles (bottom right), in which $|\vec{E}|$ is approximately 2 orders of magnitude larger than its mean value. Similar hotspots appear at different positions for different wavelengths and for different filling fractions, as

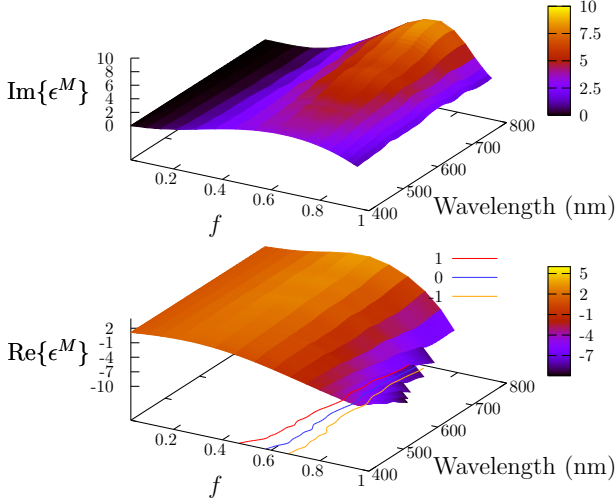


FIG. 7. Ensemble average of the imaginary part (top panel) and real part (bottom panel) of ϵ^M calculated within the RM as a function of the filling fraction f and the wavelength λ .

illustrated by the other panels of the figure. Fig.6b) shows four different hotspots for a slightly smaller f . With f even smaller Fig.6a) shows no hotspots. But, another member of the ensemble with the same f displays several as exemplified by Fig.6d). The set of hotspots for that member also change position and intensity as f grows (Figs. 6e and 6f). There are well known results on the scaling of the localized states for disordered random^{33,34} and fractal^{35,36} systems. These localized states have found applications due to the corresponding enhancement in linear and nonlinear signals. For example, SERS and KERS enhancements of 1 to 2 dozen order of magnitude have been reported.^{37,38}

The presence of hotspots in the microscopic field for filling fractions around the percolation threshold is responsible for an increased energy absorption within the conducting film, and thus to the decrease in the transmittance T as compared to that of a homogeneous film, as seen in Fig.5 for $f < f_{\max}$. This energy absorption corresponds to Joule heat that is related to the imaginary part of ϵ^M . Fig.7 displays the real and imaginary parts of the ensemble average of ϵ^M as a function of the filling fraction and of the wavelength. For $f \lesssim 1$, $h_d \approx h$, $\text{Im}\{\epsilon^M\}$ is relatively small and $\text{Re}\{\epsilon^M\} < 0$. Thus, the index of refraction $n^M = \sqrt{\epsilon^M}$ is close to an imaginary number, the film is opaque and the field decays across it by a factor $\exp\{-\text{Im}(n^M)h\}$. Therefore, as ℓ increases and h decreases the transmittance T increases. As f decreases further, $\text{Re}\epsilon^M$ becomes less negative and the field penetrates more into the film. Nevertheless, $\text{Im}\epsilon^M$ also increases and reaches a maximum for $f \approx 0.72$, thus increasing the absorption and decreasing the transmittance. For even larger ℓ and smaller f the film becomes dielectric and the transmittance increases again. This explains qualitatively the maximum and minimum transmittance observed in Fig. 5. The corresponding inflection in the transmittance is reproduced by our numerical calculation,

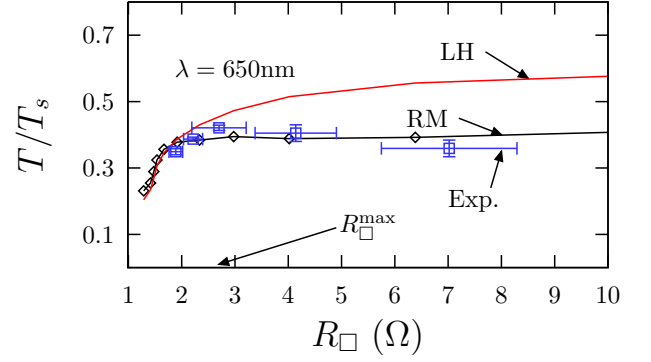


FIG. 8. Transmittance T of a film normalized to the transmittance T_s of the glass substrate vs. the sheet resistance R_{\square} for $\lambda=650$ nm. We show experimental results as well as the results from the RM calculation and results for a locally homogeneous film.

although not the actual maximum and minimum.

V. APPLICATIONS

A. Optimization of semicontinuous Ag film

An optimal transparent electrical contact would have the highest possible transmittance and the lowest possible resistance. To choose the best combination of parameters we plot T as a function of R_{\square} in Fig. 8, combining information from Figs. 4 and 5. It is clear that it is not useful to diminish the nominal width h of the film too much, as the transmittance stops increasing while the resistance does. Thus, an optimal choice would correspond to the maximum transmittance which corresponds to $T/T_s = 0.41$, $R = 2.7\Omega$, $\ell = 2$ cm, $f = 0.84$, $h = 13.8$ nm, $h_d = 16.4$ nm

B. Electro-luminescence of PS with an Ag contact

We analyze light emitting devices (LED) made of porous silicon (PS) over which Ag is sputtered to form an electrical contact. We prepare the PS sample by anodizing a crystalline p -doped Si substrate with resistivity 0.5-1.0Ωcm terminated in a (100) surface, using a well known procedure:³⁹ We immerse the Si crystal in an electrolytic solution of hydrofluoric acid, distilled water, and ethanol in proportions 1:1:2 and we apply a current with a density of 20 mA/cm² for a duration of 120 s¹² to obtain a sample with an expected porosity $p \approx 80\%$. We discard the electrolytic solution and clean the system with an ethanol bath.

If we use a diluted solution of potassium chloride as an electrolytic contact and apply a forward current with density 16 mA/cm² an electroluminescent signal is produced. We measured the normalized spectral emission with an Hitachi fluorimeter F2000 with blocked excitation source 25s after turning the current on⁴⁰. The results are displayed in Fig. 9

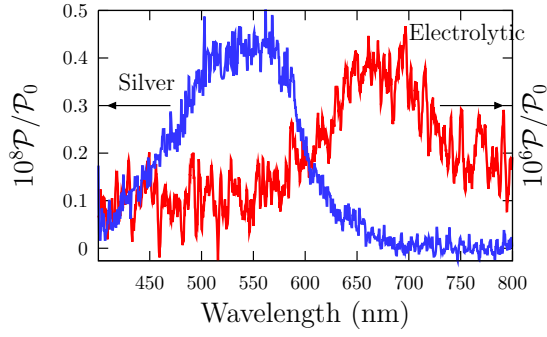


FIG. 9. Power \mathcal{P} emitted by a porous Si light emitting device as a function of wavelength λ , normalized to the electrical input power \mathcal{P}_0 . The peak on the right (right scale) corresponds to an electrolytic contact of diluted KCl and a current density of $16\text{mA}/\text{cm}^2$. The peak on the left (left scale) corresponds to a contact made of a semiconducting silver film and a current density of $20\text{mA}/\text{cm}^2$.

It is well known that luminescence of PS⁴¹ is due to the confinement of charge carriers within the pore walls, which introduces an uncertainty in the momentum that allows direct transitions that would be forbidden in bulk Si.⁴² Thus, the $\lambda = 1130$ indirect gap of bulk Si gives rise to a direct electronic transition in PS that is shifted due to quantum confinement and corresponds to the emitted emission with wavelength $\lambda = 680\text{nm}$ illustrated by the peak on the right of Fig.9 corresponding to an electrolytic contact.²¹ While the current flows, silicon oxide is progressively produced on the walls of the pores, increasing the confinement and producing a small blue shift of the maximum emission peak.³⁹ After the current had been applied for approximately 90s the electroluminescence of our sample was extinguished.

The electrical excitation of PS may also be realized with Schottky type metallic solid contacts.²¹ An advantage of metallic contacts is that the electric current doesn't produce the chemical reactions that rapidly destroys the electroluminescence when an electrolytic contact is employed, extending the life of the device. To produce a metallic contact, we use cathodic projection (sputtering) of Ag on a 0.2cm^2 masked surface of a PS sample fabricated as described above. We chose the sputtering conditions (pressure, arc current, distance of Ag target to sample, deposition time) by first sputtering onto a glass sample and selecting those conditions that yielded a film with relative transmittance $T/T_s \approx 0.2$.

Fig. 9 shows the electroluminescence spectrum of our sample with a metallic contact excited by an electric current with density density of $20\text{mA}/\text{cm}^2$. Comparing this spectrum with that corresponding to the electrolytic contact, we notice that it is strongly blue-shifted towards the central part of VIS spectra ($\approx 550\text{nm}$), but that its intensity is about two orders of magnitude smaller.

To understand the shift of the maximum of the emission spectra from $\lambda = 680$ for an electrolytic contact to $\lambda = 550$ for an Ag contact, we obtained the emission spectra from the photo-luminescence (PL) spectra of Si nano-crystals and their size dependence.⁴² The effects of confinement in the walls of

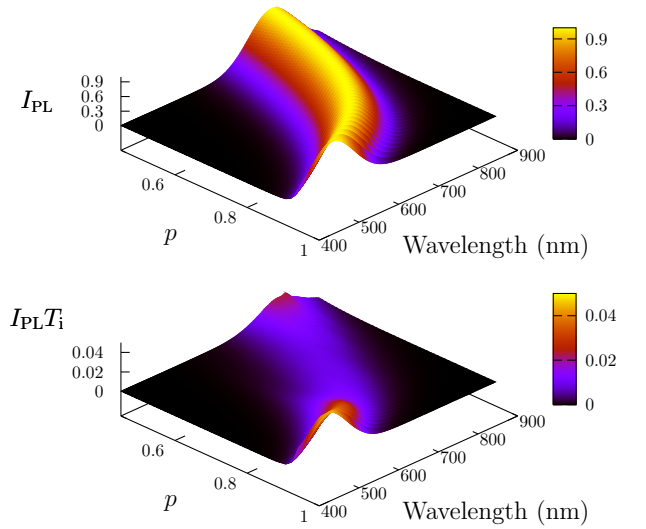


FIG. 10. Top panel: Normalized photoluminescence signal I_{PL} of porous silicon (PS) calculated as a function of porosity p and wavelength λ .³⁹ Bottom panel: Product I_{PL} of top panel with T_i for a simulated composite PS and PS permeated with Ag.

PS have been related to the effects of confinement in nano-crystals and a relation between porosity and effective size has been proposed,¹⁶ as well as analytical expressions for the shift of the emission peak with respect to size.⁴³ If the sample is kept in air there is a further blue shift due to oxidation at the surface of the pores.^{20,21} Thus, we model the intrinsic PL spectrum of PS as a Gaussian of an appropriate width centered at the energy corresponding to the porosity, and we assume that the EL emission spectrum is similar to the PL one. In the top panel of Fig.10 we show the resulting PL spectra as a function of both wavelength and porosity.³⁹

When using a solid contact, the light produced through EL is transmitted through the contact before being observed. Thus we expect that the observed EL signal should be given by the product of the emission, similar to the PL spectrum, and the optical transmittance of the system PS/contact/air. We model the contact by assuming most of the metal infiltrates the pores. We used the RM method to calculate the macroscopic dielectric response of PS modeled as a random ensemble of empty cylinders within a crystalline Si host of porosity p ,²⁷ and we also use the RM method to calculate the macroscopic dielectric response of the contact modeled as a random ensemble of Ag cylinders within the crystalline Si host, with a filling fraction given by the porosity. We calculate the transmittance T_i of the system formed by PS covered with a film of width d made up of Ag-infiltrated PS. In Fig.10 we also show the product of the intrinsic PS luminescence signal with the transmittance T_i for $d = 45\text{nm}$. Notice that the signal is suppressed about two orders of magnitude with respect to the PL spectrum and that it becomes blue shifted and more intense as the porosity increases.

Finally, we assume that the porosity in our random sample is not fixed at the nominal value $\bar{p} = 80\%$ expected from our

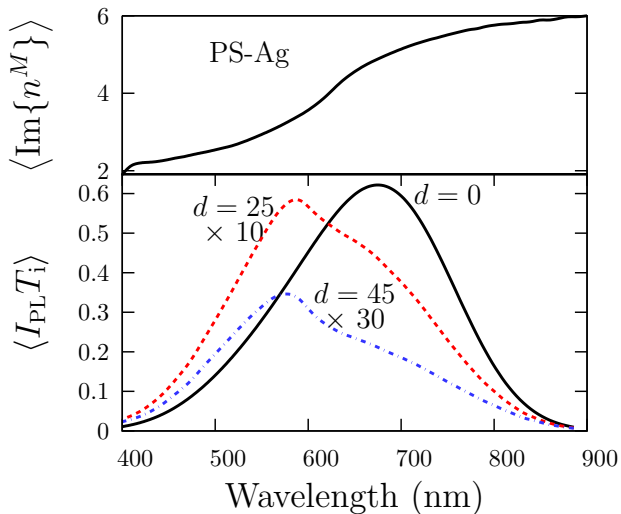


FIG. 11. Bottom panel: EL spectra calculated by multiplying the luminescence I_{PL} of PS and the transmittance T_i of the system PS/contact/air as function of wavelength λ for different values of the thickness of the contact $d = 0$ nm, 25 nm, and 45 nm. The results are averaged over porosity p assuming a Gaussian distribution of width $\sigma = 0.14$ centered at $\bar{p} = 0.8$. The curves for $d = 25$ nm and $d = 45$ nm are multiplied by 10 and 30 respectively. Top panel: imaginary part of the index of refraction n^M of the contact.

preparation procedure, but has some fluctuations. We assume p is distributed as a Gaussian of width $\sigma = 0.14$ around its average \bar{p} and. In Fig. 11 we show the corresponding EL spectra for different thicknesses d of the contact.

The curve for $d = 0$ corresponds to the absence of metal, and thus may be compared to the EL spectrum with a transparent electrolytic contact. It has a peak at 680 nm which agrees well with that in the right side of Fig. 9. The peak is slightly red shifted with respect to the nominal peak corresponding to $p = \bar{p} = 0.8$ in the top panel of Fig. 10, as the direction of its ridge is closer to that of the p axis for lower frequencies.

On the other hand, the peaks of the curves corresponding to $d = 25$ nm and $d = 45$ nm are blue shifted to 590 nm and 570 nm and are suppressed about one and two orders of magnitude respectively. The reason for the shift and the height decrease of the peaks lies in the absorption within the contact, as illustrated in the top panel of Fig. 11, which shows that the macroscopic index of refraction of the contact is large and increases with wavelength, therefore yielding a stronger suppression at the red end of the spectrum. Thus, our model of a metallic contact that partially infiltrates the pores PS is able to explain blue shift and suppression of the EL spectra observed experimentally and illustrated by the curve on the left side of Fig. 9. On the other hand, we were unable to reproduce the experimental results using a metallic semicontinuous overlayer, as in the previous sections, as a contact. Our results are not very sensitive to the width σ of the porosity distribution, but we don't get a large enough shift in the limit $\sigma \rightarrow 0$.

VI. CONCLUSIONS

We prepared Ag thin films with a height gradient by evaporation onto a tilted glass substrate. We performed ellipsometric measurements which showed that the films changed nature from locally homogeneous to semicontinuous and to an island morphology as their width diminished. We modeled the system as an ensemble of penetrable metallic cylinders occupying random uncorrelated positions, and we applied an efficient recursive formalism to obtain its macroscopic dielectric function. We fitted the ellipsometric measurements to relate the position along the sample film and the nominal height of the film to its actual height and its (area) filling fraction. We measured and analyzed with the previous fit the sheet resistance of the film and identified a percolation transition where the film resistance along the film diverges. The optical transmittance of the film was also measured and analyzed, and we obtained a deviation from the transmittance of a homogeneous film. As the film becomes narrower the transmittance increases, reaches a maximum and then it decreases until it hits a minimum and increases again, but this time as a dielectric and not a conducting film. This behavior has been attributed to the scattering of light by the inhomogeneities of the film²⁶. Nevertheless, these inhomogeneities are not expected to have a lengthscale much larger than the height of the film, much smaller than the wavelength of light, so that scattering is expected to be small⁴⁴ and the film may be characterized by a macroscopic effective permittivity.¹⁴ Our model calculation of the dielectric response captured qualitatively the behavior of the transmittance, although with smaller oscillations as the filling fraction decreases, displaying an inflection, but without an actual maximum and a minimum. We explained qualitatively the behavior of the transmittance in terms of plasmonic resonances within the film. For a range of filling fractions around the percolation threshold a series of resonances appear for which the field becomes very intense in very small regions. These hotspots are responsible for an increased energy dissipation within the film, as shown by an increase in the imaginary part of the macroscopic dielectric function of the system. We employed our results to optimize a film for use as a semitransparent contact. We also calculated the shift towards the blue and the decrease in the intensity of the electro-luminescence of porous silicon when a metallic semicontinuous contact is employed instead of an electrolytic one, and obtained agreement with experiment assuming that the metal infiltrates the pores and that the porosity has some fluctuations around its mean.

ACKNOWLEDGMENT

We acknowledge support from ANPCyT/FONCyT and UNNE through the grants PICT/2013-0696, PI-F008/2014-SGCyT, and from DGAPA-UNAM through grant No. IN113016.

- ¹ D. S. Ginley, *Handbook of Transparent Conductors* (Springer, USA, 2010).
- ² H. Ghaemi, T. Thio, D. Grupp, T. Ebbesen, and H. Lezec, *Phys. Rev. B* **58**, 6779 (1998).
- ³ S. Darmanyan and A. Zayats, *Phys. Rev. B* **67**, 035424 (2003).
- ⁴ W. Cai and V. Shalaev, *Optical Metamaterials: Fundamentals and Applications* (Springer, New York, 2009).
- ⁵ E. Cortes, W. L. Mochán, B. S. Mendoza, and G. P. Ortiz, *Phys. Stat. Sol. B* **247**, 2102 (2010).
- ⁶ W. L. Mochán, G. P. Ortiz, and B. S. Mendoza, *Opt. Express* **18**, 22119 (2010).
- ⁷ S. Brueck, *Proc. IEEE* **93**, 1704 (2005).
- ⁸ E. Martínez, M. Bellino, and G. Soler-Illia, *ACS applied materials & interfaces* **1**, 746 (2009).
- ⁹ B. O. Connor, C. Haughn, K. An, K. Pipe, and M. Shtein, *Appl. Phys. Lett* **93**, 223304 (2008).
- ¹⁰ A. I. Maarroof and G. B. Smith, *Thin Solid Films* **485**, 198 (2005).
- ¹¹ K. Seal, M. A. Nelson, and Z. C. Ying, *Phys. Rev. B* **67**, 035318 (2003).
- ¹² V. Toranzos, G. Ortiz, and R. Koropecski, in *ANALES AFA*, Vol. 22 (Asociación Física Argentina, 2010) pp. 37–41.
- ¹³ W. L. Mochán, G. Ortiz, B. S. Mendoza, and J. S. Pérez-Huerta, “Photonic,” Comprehensive Perl Archive Network (CPAN) (2016), perl package for calculations on metamaterials and photonic structures.
- ¹⁴ G. Ortiz, M. Inchaussandague, D. Skigin, R. Depine, and W. L. Mochán, *Journal of Optics* **16**, 105012 (2014).
- ¹⁵ L. C. AG Cullis and P. Calcott, *J App Phys* **82**, 909 (1997).
- ¹⁶ B. Bessaïs, H. Ezzaouia, H. Elhouichet, M. Oueslati, and R. Benaceur, *Semicond. Sci. Technol.* **11**, 1815–1820 (1996).
- ¹⁷ H. Shi, Y. Zheng, Y. Wang, and R. Yuan, *Appl. Phys. Lett.* **63**, 770 (1993).
- ¹⁸ S. Billat, F. Gaspard, R. Hérino, M. Ligeon, F. Muller, F. Romestain, and J. Vial, *Thin Solid Films* **263**, 238 (1995).
- ¹⁹ N. Koshida and H. Koyama, *Appl. Phys. Lett* **60**, 347 (1992).
- ²⁰ G. R., R. Peña-Sierra, and G. Castillo-Cabrera, *Rev. Mex. Fis.* **48**, 92 (2002).
- ²¹ P. Steiner, A. Wiedenhofer, F. Kozlowski, and W. Lang, *Thin Solid Films* **276**, 159 (1996).
- ²² P. M. Martin, *Handbook of Deposition Technologies for Films and Coatings: Science, Applications and Technology* (Elsevier, USA, 2010) p. 740.
- ²³ R. F. Bunshah, *Handbook of Deposition Technologies for Films and Coatings: Science, Applications and Technology* (Noyes Publications, USA, 1994).
- ²⁴ S. S. Cohen, *Thin Solid Films* **104**, 361 (1983).
- ²⁵ J. Zerbino, L. Pesetti, and M. Sustersic, *J. Mol. Liquids* **131-132**, 185 (2007).
- ²⁶ C. A. Bishop, *Vacuum Deposition Onto Webs, Films, and Foils* (William Andrew, New York, 2007).
- ²⁷ G. Ortiz, L. Valdez, G. López, B. Mendoza, and W. Mochán, *ANALES AFA* **22** (2010).
- ²⁸ P. B. Johnson and R. M. Christy, *Phys. Rev. B* **6**, 4370 (1972).
- ²⁹ E.D.Palik, ed., *Handbook of optical constants of solids*, Academic press handbook series (Academic, Orlando, Florida., 1985).
- ³⁰ J. C. Garland and D. B. Tanner, eds., *AIP Conference Proceeding*, AIP Conference Proceeding No. 40 (American Institute of Physics, New York, 1978).
- ³¹ J. Quintanilla, S. Torquato, and R. M. Ziff, *J. Phys. A: Math. Gen* **33**, L399 (2000).
- ³² W. L. Mochán, B. S. Mendoza, and G. P. Ortiz, in *Memorias del VI Taller sobre Metamateriales, Cristales Fotónicos, Cristales Fonónicos y Estructuras Plasmónicas* (UNISON, Hermosillo, feb. 2016, San Miguel de Allende, 2015) pp. 12–14.
- ³³ V. Shalaev, *Physics Reports* **272**, 61 (1996).
- ³⁴ V. Markel, V. Shalaev, P. Zhang, W. Huynh, L. Tay, T. Haslett, and M. Moskovits, *Phys. Rev. B* **59**, 10903 (1999).
- ³⁵ M.I.Stockman, L.N.Pandey, and T.F.George, *Phys. Rev. B* **53**, 2183 (1996).
- ³⁶ G. Ortiz and W. Mochán, *Phys. Rev. B* **67** (2003).
- ³⁷ M. Moskovits, *Rev. Mod. Phys.* **5**, 783 (1985).
- ³⁸ A. Sarychev and V. Shalaev, *Physics Reports* **335**, 275 (2000).
- ³⁹ S. Ossicini, L. Pavesi, and F. Priolo, *Light Emiting Silicon For Microphotonics*, Vol. 194 (Springer, 2003).
- ⁴⁰ V. Toranzos, R. Koropecski, R. Urteaga, and G. Ortiz, *ANALES AFA* **20**, 115 (2008).
- ⁴¹ F. Buda, J. Kohanoff, and M. Parrinello, *Phys. Rev. Lett.* **69**, 1272 (1992).
- ⁴² D. Kovalev, H. Heckler, G. Polisski, and F. Koch, *Phys. Stat. Sol. B* **215**, 871 (1999).
- ⁴³ P. Fauchet and J. von Behren, *Phys. Stat. Sol. B* **204**, R7 (1997).
- ⁴⁴ C. F. Bohren and D. R. Huffman, *Absorption and Scattering of light by small particles* (John Wiley and Sons, Inc., 1983).